Geomechanics and Engineering, *Vol. 42, No. 5 (2025) 373-383*
https://doi.org/10.12989/gae.2025.42.5.373

Mechanical response of straw fiber-soil interface subjected to freeze-thaw cycles

Chao Liu[1], Xiaojuan Yu*[1], Guizhong Xu[2], Xingyu Wu[1] and Ji Chen[2]

[1]*School of Civil Engineering, Yancheng Institute of Technology, Yancheng 224051, Jiangsu, China*
[2]*School of Architecture and Engineering, Yancheng Polytechnic College, Yancheng 224005, Jiangsu, China*

(*Received June 17, 2025, Revised August 24, 2025, Accepted August 27, 2025*)

Abstract. Natural fiber reinforcement effectively mitigates strength degradation in soils subjected to freeze-thaw cycles. Although natural fiber-soil interfacial strength plays a crucial role in controlling the behavior of fiber-reinforced frozen soils, the mechanisms underlying its evolution under freeze-thaw conditions are not yet fully understood. This study investigates straw fiber-soil interfacial strength using fiber pull-out tests, scanning electron microscopy tests, and nuclear magnetic resonance tests conducted after 0, 1, 3, 5, 10, 15, and 20 freeze-thaw cycles. The results show that interfacial strength decreases exponentially as the number of freeze-thaw cycles increases. This reduction is more pronounced at higher water contents or greater dry densities, primarily due to its positive correlation with pore development induced by freeze-thaw processes. Additionally, a calculation method is proposed for determining the critical straw fiber length in fiber-reinforced frozen soils, providing theoretical guidance for engineering applications in cold regions.

Keywords: critical straw fiber length; freeze-thaw cycle; interfacial strength; NMR analysis; SEM analysis; straw fiber-soil interface

1. Introduction

In northern China, soils are frequently exposed to freeze-thaw cycles due to pronounced seasonal and diurnal temperature variations (Bo *et al*. 2021, Yang *et al.* 2024). These cycles progressively degrade the mechanical properties of soils, resulting in a significant reduction in strength. Such deterioration poses a serious risk to the safety and long-term stability of geotechnical structures in the region, often manifesting as foundation settlement, slope failure, and pavement damage (Tang *et al*. 2020, Cheng *et al*. 2021, Bo *et al*. 2021, Yu *et al*. 2025). Therefore, it is essential to investigate and develop effective techniques to improve the geotechnical behavior of soils subjected to freeze-thaw conditions.

Fiber reinforcement, through the incorporation of synthetic fibers such as steel, carbon, and polypropylene fibers, has proven effective in enhancing the engineering properties of frozen soils (Kravchenko *et al*. 2019, Ali *et al*. 2020, Kumar *et al*. 2020, Kakroudi *et al*. 2024, Bozyigit 2025). A range of laboratory investigations, including unconfined compressive strength, direct shear, tensile, and CBR tests, have consistently demonstrated that fiber inclusion not only mitigates strength loss but also improves the ductility of frozen soils (Orakoglu and Liu 2017, Li *et al.* 2018, Bahrami and Marandi 2020, Yan *et al.* 2021, Vakili *et al.* 2022, Oulapour *et al.* 2025). Compared with synthetic fibers, natural fibers, such as jute, bagasse, coir, and chicken quill fibers, offer advantages including low cost, environmental sustainability, and wide availability. Several studies have investigated the reinforcement of frozen soils using these natural fibers, reporting significant improvements in both strength and ductility under freeze-thaw conditions relative to untreated soils (Güllü and Khudir 2014, Dang *et al*. 2016, Zaimoglu *et al*. 2016, Liu *et al*. 2020). However, the underlying reinforcing mechanisms of natural fibers in frozen soils remain insufficiently understood.

Among the various factors influencing the reinforcing mechanisms, the interfacial interaction between the fiber and surrounding soil is considered critical (Hejazi *et al*. 2012, Zhu *et al*. 2014, Yu *et al*. 2025). Of the various experimental methods available, the single-fiber pull-out test is the most widely used for evaluating interfacial behavior due to its simplicity and broad applicability (Toufigh *et al*. 2014, Monazami and Gupta 2022). Extensive research has been conducted to investigate factors influencing interfacial behavior, including fiber shape (Tang *et al*. 2016, Vincenzini *et al*. 2021), fiber surface roughness (Singh *et al*. 2004, Yao *et al*. 2024), fiber embedment length (Shannag *et al*. 1997, Singh *et al*. 2004, Li *et al*. 2018), loading rate (Ji *et al*. 2018), soil water content (Tang *et al*. 2010, Kafodya and Okonta 2021), and soil dry density (Tang *et al*. 2010, Vincenzini *et al*. 2021). In particular, fiber embedment length has been a subject of extensive research. Numerous pull-out tests have shown that embedment length significantly affects both the interfacial shear area and the debonding-slip process (Lee *et al*. 2010, Sun *et al*. 2024). Liu *et al*. (2020) reported that

*Corresponding author, Professor
E-mail: yuxiaojuan@ycit.edu.cn

ISSN: 2005-307X (Print), 2092-6219 (Online)

Table 1 Physical and mechanical properties of the tested soil

Liquid limit	Plastic limit	Maximum dry density	Optimum water content	Cohesion	Angle of internal friction	Particle size distribution (mm)		
						<0.005	0.005-0.075	>0.075
30.2%	17.2%	1.73 g/cm3	18.2%	18.0 kPa	24.2°	21.7%	76.5%	1.8%

Table 2 Physical and mechanical properties of the cotton straw fiber

Length	Average diameter	Unit weight	Elongation at break	Tensile strength	Modulus of elasticity
100 mm	0.1 mm	1.53 g/cm^3	6.2-7.8 %	102.5 MPa	4860 MPa

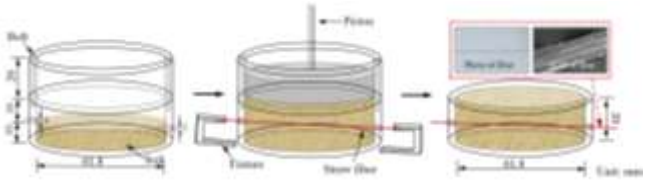

(a) Sample preparation process

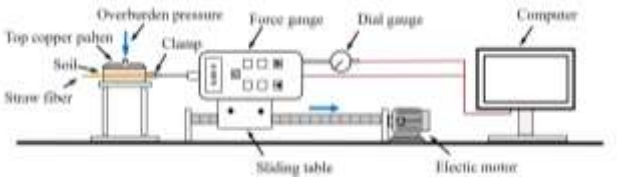

(b) Schematic of the single-fiber pull-out test apparatus

Fig. 1. Single-fiber pull-out test

although embedment length influences the load-displacement curves in single-fiber pull-out tests, it has little effect on the interfacial peak or residual strength. Consistently, Singh *et al*. (2004) found that while the peak pull-out load increases roughly linearly with embedment length, the interfacial shear strength does not vary significantly across different lengths. Nevertheless, studies specifically addressing the mechanical behavior of the fiber-soil interface under freeze-thaw conditions remain limited.

This study investigated the strength characteristics of the straw fiber-soil interface under freeze-thaw cycles. Single-fiber pull-out tests were conducted to evaluate interfacial strength, and changes in interfacial properties were further analyzed using scanning electron microscopy (SEM) and nuclear magnetic resonance (NMR) tests. In addition, a method for calculating the critical straw fiber length in fiber-reinforced frozen soil was proposed. The findings of this study provide theoretical support for the engineering design of straw fiber-reinforced soil in cold regions.

2. Materials and methods

2.1 Materials

The soil used in this study was collected from a construction site in Dongtai, Jiangsu Province, China. After collection, it was air-dried and passed through a 2 mm mesh. Its physical and mechanical properties are summarized in Table 1. The maximum dry density and optimum water content are 1.73 g/cm^3 and 18.2%, respectively. Cotton straw fiber, an agricultural by-product, was used as the reinforcing material. Its physical and mechanical properties, as provided by the manufacturer, are listed in Table 2. The fiber has a density of 1.53 g/cm^3 and a tensile strength of 102.5 MPa.

2.2 Fiber pull-out tests

This study determines the strength parameters of the fiber-soil interface, including the interfacial peak strength, cohesion, and friction angle, through single-fiber pull-out tests. In contrast, conventional direct shear or triaxial tests assess the macroscopic shear strength of fiber-reinforced soil. It is important to emphasize that the macroscopic strength of fiber-reinforced soil is largely governed by the properties of the fiber-soil interface. Therefore, the interfacial strength parameters obtained in this study primarily reflect the mechanical behavior at the mesoscopic scale and provide a mechanistic basis for interpreting the macroscopic shear behavior of fiber-reinforced soil, thereby contributing to a better understanding of its overall mechanical performance. Table 3 outlines the experimental design for the fiber pull-out tests. Tests were conducted at four water contents (14.2%, 16.2%, 18.2%, and 20.2%) and four dry densities (1.4, 1.5, 1.6, and 1.7 g/cm^3). The testing procedure was as follows (Fig. 1(a)): First, dry soil was mixed with water to achieve the target of a modified portable low-pressure consolidation device, a sliding table

Table 3 Experimental design for the fiber pull-out tests

Sample no.	Water content (%)	Dry density (g/cm^3)	Vertical stress (kPa)	Number of freeze-thaw cycles
S1	18.2	1.7	0	0, 1, 3, 5, 10, 15, 20
S2	18.2	1.7	50	0, 1, 3, 5, 10, 15, 20
S3	18.2	1.7	100	0, 1, 3, 5, 10, 15, 20
S4	18.2	1.7	150	0, 1, 3, 5, 10, 15, 20
S5	14.2	1.7	0	0, 1, 3, 5, 10, 15, 20
S6	16.2	1.7	0	0, 1, 3, 5, 10, 15, 20
S7	20.2	1.7	0	0, 1, 3, 5, 10, 15, 20
S8	18.2	1.4	0	0, 1, 3, 5, 10, 15, 20
S9	18.2	1.5	0	0, 1, 3, 5, 10, 15, 20
S10	18.2	1.6	0	0, 1, 3, 5, 10, 15, 20

module driven by an electric motor, a force gauge, and a dial gauge. The sample was placed in the consolidation device, which allowed the application of vertical stresses of 0, 50, 100, and 150 kPa. The free end of the fiber was connected to the force gauge using a custom-designed clamp to ensure proper horizontal alignment. The pull-out force was applied at a constant speed of 1 mm/min, controlled by an electric motor mounted on the sliding table. Throughout the test, the force gauge and dial gauge continuously recorded the pull-out load and corresponding displacement.

2.3 SEM and NMR tests

Microstructural observations were performed using SEM. Samples were vacuum freeze-dried, sputter-coated with a thin gold layer to improve electrical conductivity, and mounted on the SEM stub. Imaging was carried out at an accelerating voltage of 10 kV. In addition, the pore size distribution was analyzed using NMR techniques. Samples were first vacuum-saturated, after which the transverse relaxation time (T_2) distribution of the saturated samples was measured. The pore structure of the sample is related to the T_2 distribution according to the following relationship (Tian *et al*. 2014)

$$R = 2\rho_2 T_2 \tag{1}$$

Where R is the pore radius and ρ_2 is the surface relaxivity of the sample. In this study, the measured surface relaxivity was ρ_2=10 μm/s.

3. Test results

3.1 Effect of freeze-thaw cycles on pull-out behavior

Fig. 2 illustrates the pull-out load-displacement responses of the samples subjected to different numbers of freeze-thaw cycles under vertical stresses of 0, 50, 100, and 150 kPa. The pull-out behavior can be categorized into three distinct stages. In the initial stage, the pull-out load increased almost linearly with displacement, with no relative movement occurring between the fiber and the surrounding soil. The resistance during this stage primarily resulted from interfacial cohesion and friction, while the fiber underwent elastic deformation, accumulating strain energy at the fiber-soil interface. In the second stage, debonding at the interface began once the peak pull-out load was reached. The release of stored strain energy caused relative slippage and a sharp decrease in pull-out load. In the final stage, as displacement continued, the pull-out load stabilized at a lower residual level. This overall load-displacement trend is consistent with findings reported by Tang *et al*. (2010) and Zhu *et al*. (2014). Although the number of freeze-thaw cycles and the magnitude of applied vertical stress influence the peak pull-out load, the general shape of the response curves remains largely unchanged, indicating that these factors do not fundamentally alter the underlying pull-out behavior.

As shown in Fig. 2(a), the peak pull-out loads for 0, 1, 3, 5, 10, 15, and 20 freeze-thaw cycles were approximately 1.58, 1.15, 1.00, 0.94, 0.90, 0.88, and 0.87 N, respectively, with corresponding displacements of approximately 6.2, 6.0, 5.8, 5.8, 5.6, 5.4, and 5.0 mm. Both the peak load and the associated displacement decrease gradually with an increasing number of freeze-thaw cycles, indicating progressive weakening of the fiber-soil interface. This weakening suggests that repeated freeze-thaw cycles increase the susceptibility of the interface to shear failure, even under lower pull-out loads and reduced displacements. Comparing Fig. 2(a) through Fig. 2(d), which correspond to vertical stresses of 0, 50, 100, and 150 kPa, respectively, the peak pull-out loads after 20 freeze-thaw cycles were 0.87, 0.96, 1.21, and 1.38 N. These values represented reductions of 44.94%, 42.58%, 39.88%, and 38.57%, respectively, relative to the peak values under the same vertical loads without freeze-thaw cycles. These results demonstrate that increasing vertical stress can partially mitigate the loss in pull-out load induced by freeze-thaw cycling.

Based on Fig. 2, the interfacial peak strength (τ_f), interfacial cohesion (c), and interfacial friction angle (φ) are calculated using the following equations (Tang *et al*. 2010, Xu 2022)

$$\tau_f = \frac{F_{max}}{\pi dl} \tag{2}$$

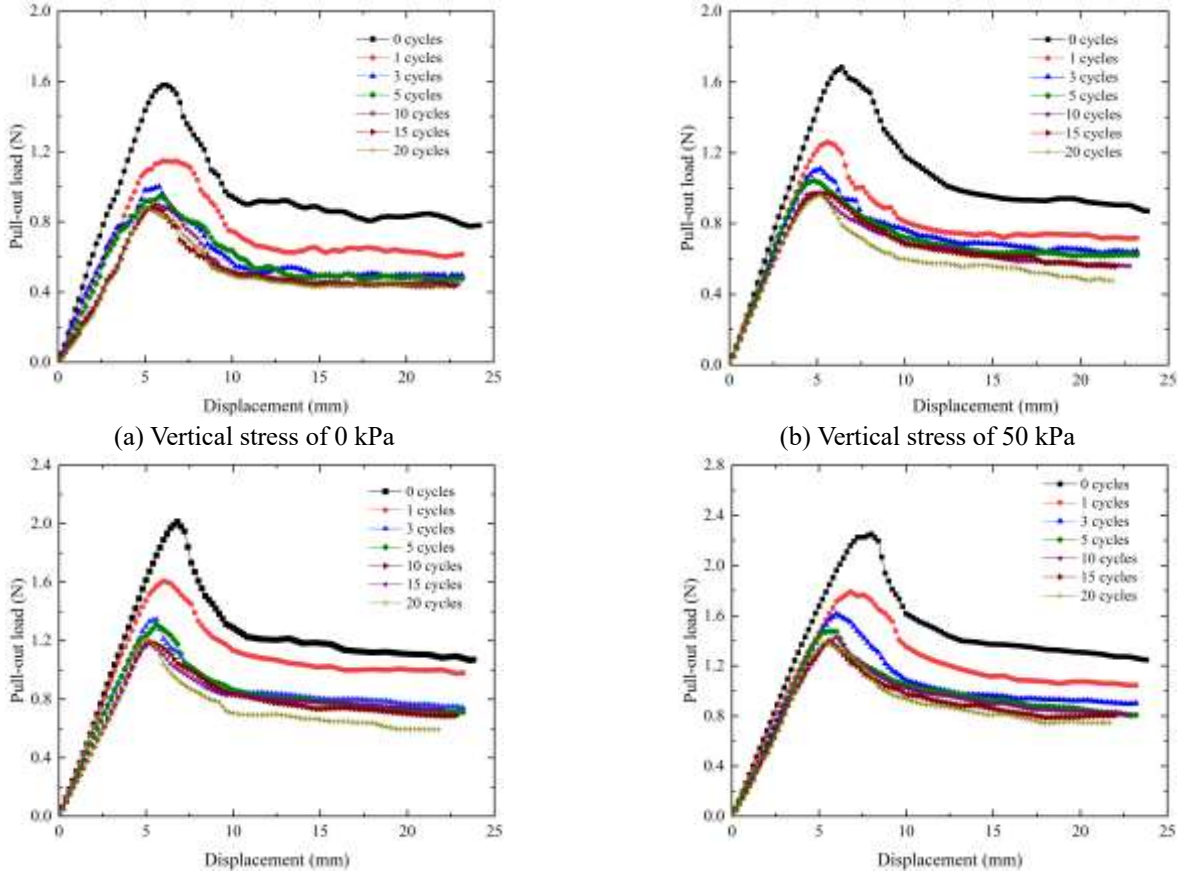

(a) Vertical stress of 0 kPa (b) Vertical stress of 50 kPa

(c) Vertical stress of 100 kPa (d) Vertical stress of 150 kPa

Fig. 2 Pull-out load-displacement curves under freeze-thaw conditions

$$\tau_f = c + \delta \tan\varphi \tag{3}$$

Where F_{max} is the peak pull-out load; d is the fiber diameter; l is the fiber embedded length; δ is the vertical stress. In Fig. 3, the interfacial cohesion corresponding to 0, 1, 3, 5, 10, 15, and 20 freeze-thaw cycles was 78.87, 57.20, 49.22, 47.08, 43.92, 43.57, 43.31 kPa, respectively. A pronounced reduction of 40.30% in interfacial cohesion was observed within the first five freeze-thaw cycles. Between the 5th and 10th cycles, the interfacial cohesion further decreased by 6.71%, while from the 10th to the 20th cycle, the decrease was limited to only 1.38%. These results indicate a trend of rapid initial degradation, followed by a gradual reduction and eventual stabilization. A similar trend is observed for the interfacial friction angle with increasing freeze-thaw cycles. To quantitatively describe this behavior, the following semi-empirical equation is proposed

$$F_N = F_0\left(a\left(e^{-N/b}-1\right)+1\right) \tag{4}$$

Where F_N is the value of a given parameter (e.g., interfacial cohesion, interfacial friction angle, or interfacial strength) after N freeze-thaw cycles; F_0 is the corresponding value without freeze-thaw cycles; N is the number of freeze-thaw cycles; a and b are fitting parameters that characterize the shape of the degradation curve. In this study, the fitting values of a and b were 0.43 and 1.11 for interfacial cohesion, and 0.25 and 4.40 for the interfacial friction angle, respectively. The high coefficient of determination (R^2>0.98) indicates that the proposed equation provides an excellent fit to the experimental data and reliably captures the relationship between the variables. By fitting results from a limited number of freeze-thaw cycles, the parameters in Eq. (4) can be determined, enabling prediction of fiber-soil interfacial strength under arbitrary numbers of cycles. Laboratory tests indicate that the fiber-soil interface parameters undergo pronounced degradation during the initial freeze-thaw cycles, demonstrating the significant impact of initial freeze-thaw cycles on the interface. While field conditions differ from laboratory settings, with milder temperature fluctuations, lower freeze-thaw intensity, and more complex soil boundary conditions, these differences primarily influence the number of cycles required for the interface parameters to reach their residual values rather than altering the overall trend of gradual deterioration followed by stabilization. Consequently, laboratory studies offer a reliable basis for understanding the degradation patterns of interface parameters in engineering applications. The degradation models developed from laboratory experiments can be used to estimate the evolution of in situ interface properties, providing valuable guidance for design. Moreover, since interface parameters tend to stabilize after a limited number of cycles, these stabilized values can be adopted as the design strength of the fiber-soil interface in cold-region projects. This approach not only offers a more

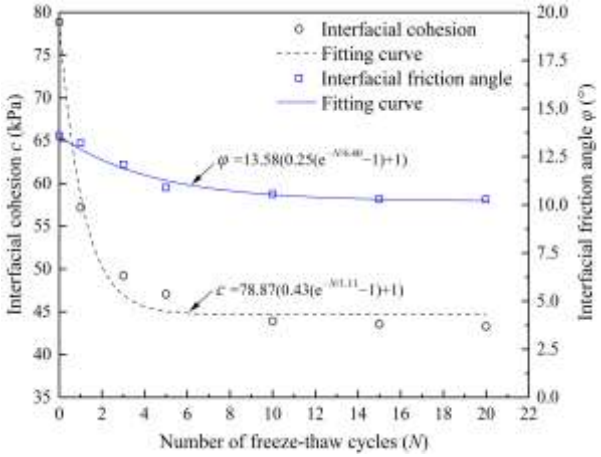

Fig. 3 Interfacial cohesion and friction angle under freeze-thaw conditions

accurate representation of long-term structural performance but also enhances the durability and safety of engineering works.

3.2 Effect of freeze-thaw cycles on interfacial strength under varying water contents

Fig. 4(a) illustrates the fiber pull-out load-displacement curves for samples with varying water contents, both before and after freeze-thaw cycles. In the absence of freeze-thaw cycling (0 cycles), increasing the water content from 14.2% to 20.2% resulted in a significant decrease in the interfacial peak load from 2.29 N to 0.69 N, a reduction of 69.86%. After 20 freeze-thaw cycles, the same increase in water content resulted in a reduction of the peak load from 1.79 N to 0.42 N, a 76.54% decrease. These results demonstrate that higher water content significantly weakens the pull-out resistance at the fiber-soil interface, regardless of freeze-thaw exposure. This weakening is primarily attributed to the reduction in matric suction between the fiber surface and soil particles as water content increases. The decrease in capillary forces weakens the interfacial bond, lowering the frictional resistance required for particle displacement during pull-out. Moreover, excess water forms a thicker water film at the interface, which acts as a lubricant and further reduces frictional resistance, thereby weakening the interfacial bond strength.

Fig. 4(b) illustrates the variation in fiber-soil interfacial peak strength with increasing freeze-thaw cycles. For samples with identical water content, the interfacial peak strength exhibited an exponential decay with the number of freeze-thaw cycles. This trend aligns with the observed reductions in both interfacial cohesion and interfacial friction angle (Fig. 3). The data are fitted using Eq. (4), and all coefficients of determination (R^2) exceed 0.96, indicating a strong correlation between the proposed semi-empirical equation and the test results. Prior to freeze-thaw cycles, the interfacial peak strengths at water contents of 14.2%, 16.2%, 18.2%, and 20.2% were 121.26, 96.02, 81.42, and 35.91 kPa, respectively. After 20 freeze-thaw cycles, the corresponding values decreased to 92.72, 59.97, 45.44, and 19.90 kPa, representing reductions of 23.54%, 37.54%, 44.19%, and 44.59%, respectively, relative to the

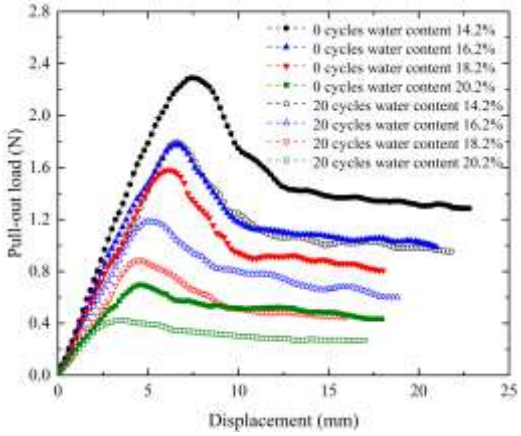

(a) Pull-out load-displacement curves

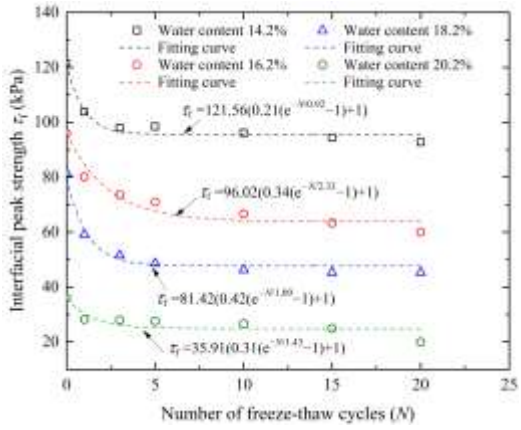

(b) Interfacial peak strength curves

Fig. 4 Effects of freeze-thaw cycles on interfacial strength under varying water contents

initial strengths. These findings suggest that higher water content significantly accelerates the deterioration of fiber-soil interfacial peak strength under freeze-thaw conditions.

3.3 Effect of freeze-thaw cycles on interfacial strength under varying dry densities

Fig. 5(a) presents the pull-out load-displacement curves of samples with varying dry densities, both before and after freeze-thaw cycles. Regardless of freeze-thaw cycles, samples with higher dry densities consistently exhibited greater pull-out loads compared to those with lower dry densities, indicating an increase in the resistance required to initiate interfacial failure. Furthermore, the displacement corresponding to the peak pull-out load increased with dry density, suggesting an enhanced deformation capacity prior to failure. This improvement in interface behavior can be attributed to the influence of dry density on the fiber-soil interaction. Higher dry density reduces the internal void ratio, resulting in increased effective contact between the particles and the fiber surface. Moreover, the compaction effort associated with higher dry densities may lead to partial embedding of soil particles into the fiber surface, promoting mechanical interlocking and further strengthening the fiber-soil interfacial bond (Tang *et al.* 2016).

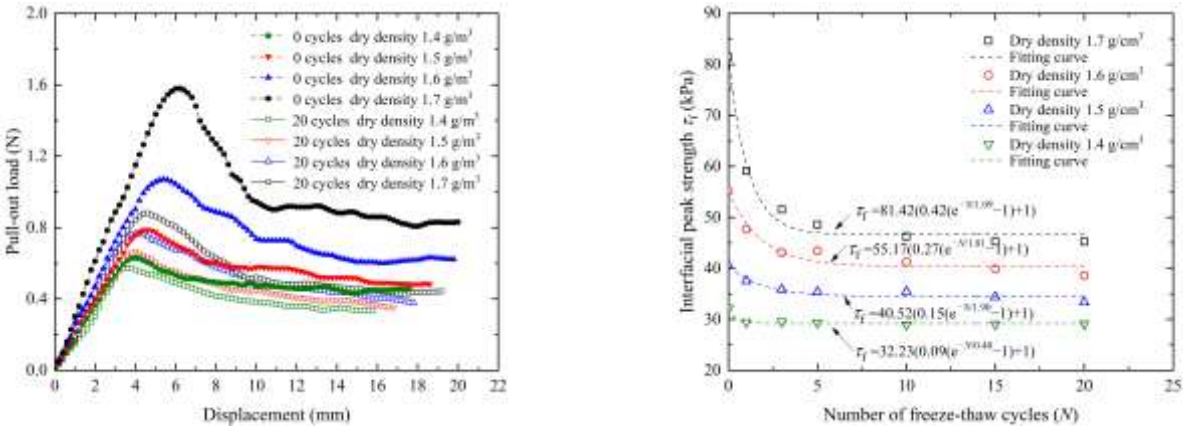

(a) Pull-out load-displacement curves (b) Interfacial peak strength curves

Fig. 5 Effects of freeze-thaw cycles on interfacial strength under varying dry densities

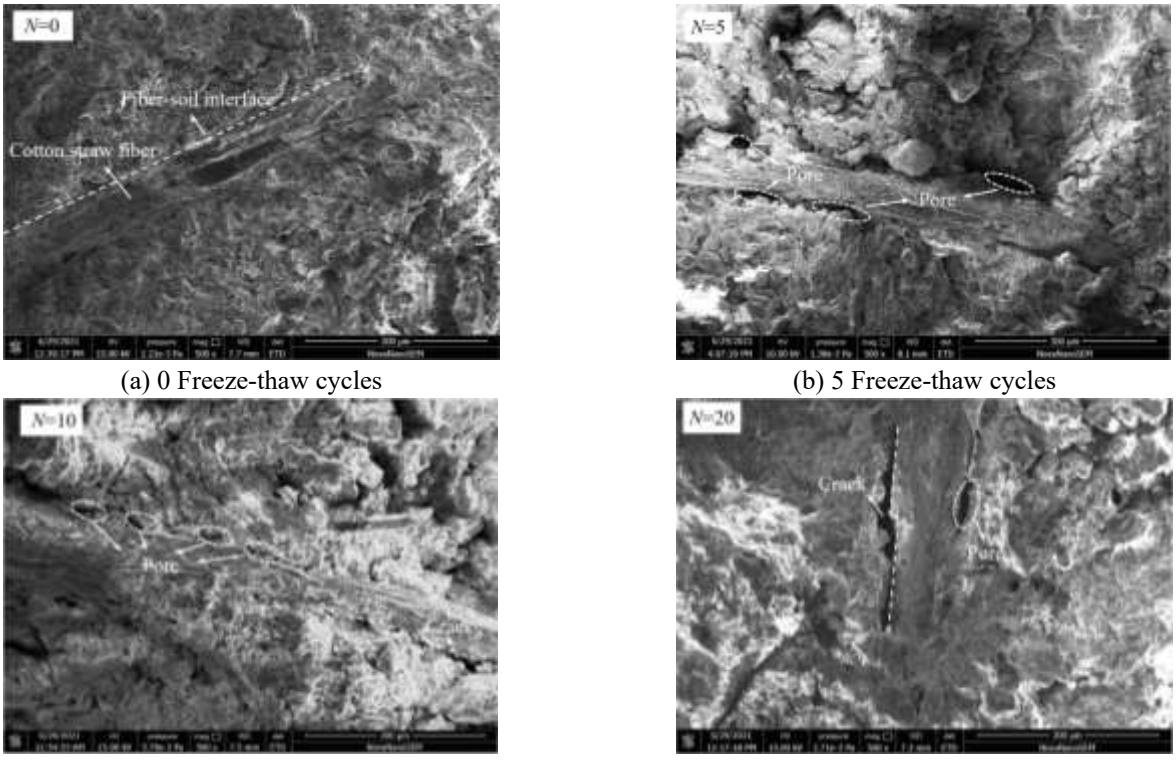

(a) 0 Freeze-thaw cycles (b) 5 Freeze-thaw cycles

(c) 10 Freeze-thaw cycles (d) 20 Freeze-thaw cycles

Fig. 6 SEM images of fiber-soil interfaces subjected to freeze-thaw cycles

Fig. 5(b) illustrates the relationship between fiber-soil interfacial peak strength and dry density under freeze-thaw conditions. The interfacial peak strength decreased exponentially with an increasing number of freeze-thaw cycles. Prior to freeze-thaw cycles, the interfacial peak strengths at dry densities of 1.4, 1.5, 1.6, and 1.7 g/cm³ were 32.25, 40.52, 55.17, and 81.42 kPa, respectively. After 20 freeze-thaw cycles, the corresponding values decreased to 29.12, 33.35, 38.56, and 45.23 kPa, corresponding to reductions of 9.71%, 17.69%, 30.11%, and 44.45%, respectively, relative to the initial strengths. These findings indicate that freeze-thaw cycling has a more pronounced degrading effect on the interfacial peak strength of samples with higher dry densities.

4. Discussion

4.1 Interaction mechanism of fiber-soil interface under freeze-thaw cycles

Fig. 6(a)-6(d) display SEM images of the sample S1 after 0, 5, 10, and 20 freeze-thaw cycles, respectively, at a magnification of 500×. As shown in Fig. 6(a), prior to freeze-thaw cycles, the fiber was tightly embedded within the soil matrix, exhibiting a compact interface with minimal voids. This close contact ensured strong interfacial bonding, thereby providing high pull-out resistance during mechanical testing. As freezing occurred, water at the fiber-

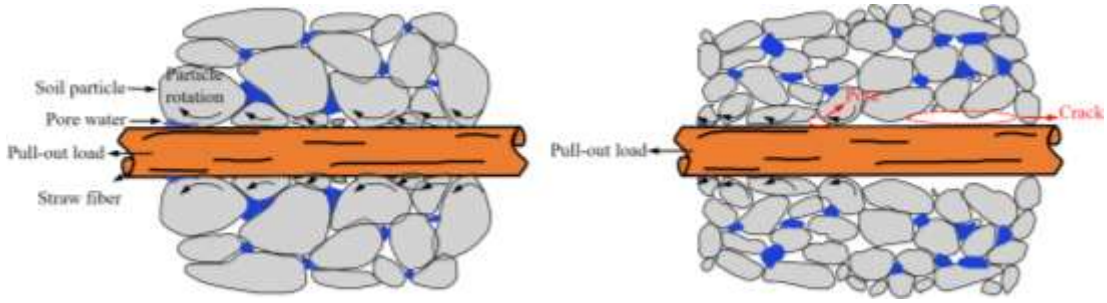

(a) Before freeze-thaw cycles (b) After freeze-thaw cycles

Fig. 7 Schematic of pull-out behavior under freeze-thaw cycles

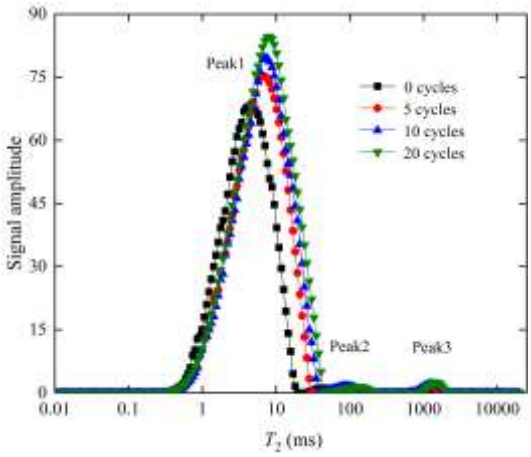

Fig. 8 Transverse relaxation time distribution under freeze-thaw cycles

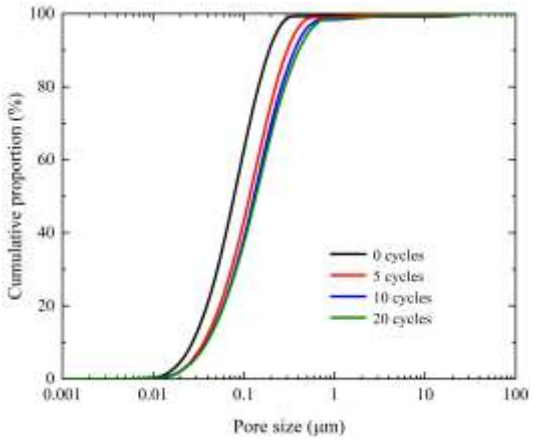

Fig. 9 Pore size distribution curves under freeze-thaw cycles

soil interface froze and expanded, increasing the size of interfacial pores, as illustrated in Fig. 6(b). Additionally, thermal gradients generated during cyclic freezing and thawing induced water migration and led to the rearrangement of soil particles. These combined effects progressively disrupted the initial compact configuration, resulting in a looser interface, increased porosity, and eventually visible cracking, as observed in Fig. 6(c) and 6(d). The reduction in effective contact area between the fiber and soil led to a decrease in both interfacial cohesion and friction angle, thereby weakening the pull-out resistance and degrading the overall interfacial bonding. These microstructural observations, along with the schematic representation of the fiber pull-out mechanism (Fig. 7), highlight the progressive deterioration of the fiber-soil interface under freeze-thaw conditions. The findings are consistent with the reduction in interfacial strength shown in Fig. 2.

Fig. 8 presents the transverse relaxation time distribution curves of the sample S1 after 0, 5, 10, and 20 freeze-thaw cycles. Prior to freeze-thaw cycling, the T_2 curve displayed three distinct peaks. Peak 1, exhibiting the highest signal amplitude, corresponded to relaxation times primarily within the range of 0.3-20 ms. Peak 2 appeared between 22 and 70 ms, while Peak 3 was observed in the range of 600-1000 ms. After 5, 10 and 20 freeze-thaw cycles, all peaks shifted toward longer relaxation times, suggesting an overall increase in pore size. Simultaneously, peak amplitudes rose, reflecting an increase in pore volume and number. The most pronounced shifts and amplitude growth occurred during the first five cycles, suggesting rapid pore development and underscoring the strong initial impact of freeze-thaw processes on the fiber-soil interface. Between 5 and 10 cycles, both the degree of peak shift and the amplitude increase diminished, indicating a deceleration in microcrack propagation and a progressive trend toward dynamic equilibrium at the interface. Eventually, a relatively stable contact condition was established between the fiber and the surrounding soil matrix. These observations are consistent with the exponential reduction in fiber-soil interfacial strength subjected to freeze-thaw cycles, as illustrated in Fig. 3

Based on the transverse relaxation time distributions shown in Fig. 8, the corresponding pore size distribution curves were calculated using Eq. (1), as presented in Fig. 9. For comparative analysis, pores were categorized into three groups: small pores ($R \leq 0.1$ μm), medium pores (0.1 μm < $R \leq 1$ μm), and large pores ($R > 1$ μm) (Deng *et al*. 2015). Before freeze-thaw cycling, the proportions of small, medium, and large pores were 61.61%, 38.17%, and 0.22%, respectively. After 20 cycles, these proportions changed to 36.31%, 62.34%, and 1.35%, respectively. This evolution indicates a gradual reduction in the proportion of small pores and a corresponding increase in medium and large pores with increasing freeze-thaw cycles. These changes are primarily driven by the cyclic phase transitions of water within the soil matrix. During freezing, the expansion of

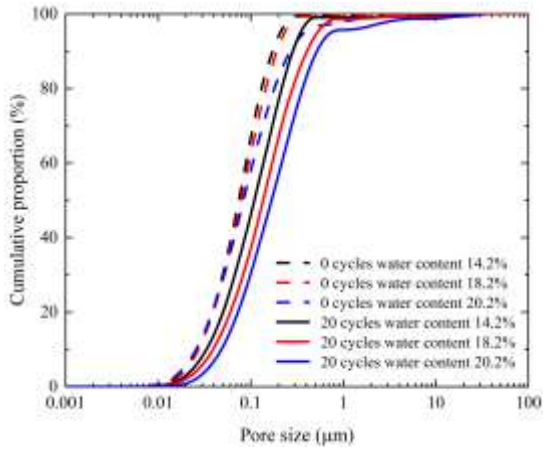

Fig. 10 Effect of water content on pore size distribution under freeze-thaw cycles

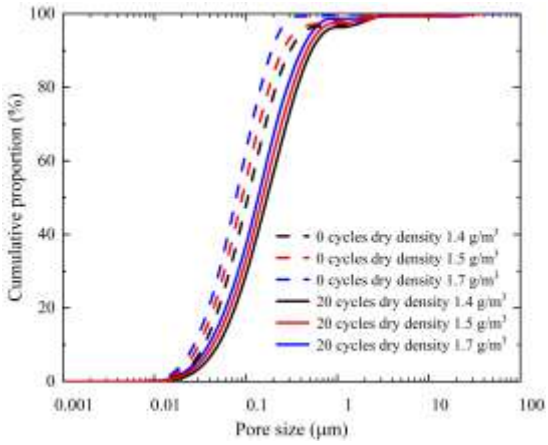

Fig. 11 Effect of dry density on pore size distribution under freeze-thaw cycles

water exerts pressure on pore walls and induces structural damage, thereby reducing the volume of small pores. Simultaneously, particle rearrangement promotes the transformation of small pores into larger ones. The repeated expansion and contraction further accelerates the formation and enlargement of pores. As a result, the effective contact area at the fiber-soil interface decreases, leading to a reduction in interfacial strength.

4.2 Mechanism of freeze-thaw effects on pull-out behavior under varying water contents

Fig. 10 illustrates the pore size distribution of samples with water contents of 14.2%, 18.2%, and 20.2%, both before and after 20 freeze-thaw cycles. Prior to freeze-thaw cycling, the proportions of small pores in these samples were 65.74%, 61.61%, and 57.08%, respectively. Corresponding proportions of medium pores were 33.80%, 38.17%, and 40.86%, while large pores accounted for 0.46%, 0.22%, and 2.06%. As water content increases, the proportion of small pores decreases, while those of medium and large pores increase. This trend is attributed to the greater pore occupancy by water, which enhances particle lubrication and facilitates particle slippage and rearrangement among soil particles, thereby promoting the conversion of small pores into larger ones (Liu *et al*. 2020). In addition, higher water content lowers matric suction, weakening interparticle adhesion and increasing interparticle spacing, which further contributes to the formation and enlargement of pores.

After 20 freeze-thaw cycles, the proportion of small pores in samples with water contents of 14.2%, 18.2%, and 20.2% decreased by 20.47%, 25.30%, and 27.40%, respectively, relative to their initial values. Correspondingly, the proportion of medium pores increased by 20.01%, 24.17%, and 25.19%, while those of large pores increased by 0.47%, 1.13%, and 2.21%. At a constant dry density, the frost heave potential decreases with lower water content due to increased matric suction and reduced ice formation, which collectively weakens frost damage and limits the development of pore structures. In contrast, higher water content intensifies volumetric expansion during freezing, resulting in more pronounced pore enlargement. These findings confirm that higher water content enhances pore evolution during freeze-thaw processes, which in turn accelerates the degradation of interfacial strength, as also evidenced in Fig. 4.

4.3 Mechanism of freeze-thaw effects on pull-out behavior under varying dry densities

Fig. 11 presents the pore size distribution curves for samples with dry densities of 1.4, 1.5, and 1.7 g/cm³ before and after 20 freeze-thaw cycles. Prior to freeze-thaw cycling, the proportions of small pores in these samples were 46.94%, 53.66%, and 61.61%, respectively. The corresponding proportions of medium pores were 49.87%, 44.38%, and 38.17%, while large pores accounted for 3.19%, 1.96%, and 0.22%. A higher dry density is associated with an increased proportion of small pores and a decreased proportion of medium and large pores. This trend can be attributed to the effects of compaction, which reduce interparticle spacing and compress or eliminate larger voids, thereby producing a denser soil structure (Chen 2018, Bag and Jadda 2021). Moreover, increased compaction enhances the number of interparticle contact points, promoting the formation of closed small pores and further decreasing the prevalence of medium and large pores (Li *et al*. 2018).

After 20 freeze-thaw cycles, the proportion of small pores in samples with dry densities of 1.4, 1.5, and 1.7 g/cm³ decreased to 28.28%, 32.29%, and 36.31%, respectively, while the proportions of medium pores increased to 68.07%, 65.21%, and 62.34% and those of large pores increased to 3.65%, 2.50%, and 1.35%, respectively. These results indicate that freeze-thaw cycles promote the conversion of small pores into medium and large pores. In densely compacted soils, the tight structure makes them more vulnerable to frost heave-induced particle displacement, leading to the collapse or coalescence of small pores (Li *et al.* 2020, Wang *et al*. 2020, Cheng *et al*. 2021, Yang *et al.* 2024). Moreover, stress concentration around existing small pores renders them unstable under repeated freeze-thaw cycles, eventually merging into larger voids. As pores expand and multiply, the effective contact

area between the fiber and the surrounding soil decreases, leading to a decline in interfacial strength, as illustrated in Fig. 5.

5. Engineering applications

In practical engineering applications, straw fibers have been extensively studied as sustainable reinforcement materials to improve the mechanical properties of soils subjected to freeze-thaw cycles (Hejazi *et al*. 2012, Cheng *et al*. 2021, Bo *et al*. 2021, Xu 2022). For the rational and efficient use of such materials under these environmental conditions, it is crucial to determine the critical fiber length, which serves as a key design parameter. According to the authors' previous study (Yu *et al*. 2025), the tensile strength of straw fibers decreases with increasing freeze-thaw cycles due to the deterioration of cellulose, lignin, hemicellulose, and other organic constituents. This decrease follows an exponential decay pattern, which can be described by the equation: $R_f = g \cdot e^{-N/h} + m$. The mechanical behavior of straw fiber-reinforced frozen soils is analyzed by assuming that the fibers are laid linearly within the soil matrix and that tensile cracking of the soil occurs at the midpoint of each fiber, as illustrated in Fig. 12. The critical straw fiber length for the *N*-th freeze-thaw cycle (l_{CN}) is defined as the length at which the tensile load at the midpoint reaches the fiber's ultimate tensile strength, and is calculated using Eq. (5). To ensure engineering safety and structural reliability, the maximum value of the critical straw fiber length over *N* freeze-thaw cycles (l_{CNmax}) should be adopted for design purposes, as given by Eq. (6).

$$l_{CN} = \frac{R_f d}{2\tau_f} = \frac{(g \cdot e^{-N/h} + m) d}{2\tau_0 \cdot \left(a(e^{-N/b} - 1) + 1\right)} \tag{5}$$

$$l_{CNmax} = max\left(l_{C1}, l_{C2}, l_{C3} \cdots\cdots, l_{CN}\right) \tag{6}$$

Where R_f is the tensile strength of a single fiber; d is the fiber diameter; τ_f is the interfacial peak strength between the fiber and the surrounding soil; τ_0 is the interfacial peak strength without freeze-thaw cycles; N is the number of freeze-thaw cycles; g, h, and m are the fitting coefficients describing the degradation of fiber tensile strength under freeze-thaw conditions; a and b are the fitting parameters characterizing the evolution of fiber-soil interfacial strength with freeze-thaw cycling.

The maximum critical straw fiber length l_{CNmax} can be calculated using Eqs. (5) and (6). The values of l_{CNmax} in samples S1 through S10 are determined to be 51.3, 47.1, 38.2, 32.2, 25.7, 36.9, 97.3, 85.9, 70.2, and 59.3 mm, respectively. When the actual fiber length is less than the critical value, fiber pull-out occurs during the failure of the reinforced frozen soil. If the actual fiber length equals the critical length, fiber rupture may occur only when the tensile crack coincides precisely with the fiber midpoint; otherwise, pull-out occurs from the side with the shorter embedded length. When the actual fiber length exceeds the critical length, fiber rupture becomes possible during the failure of the reinforced frozen soil. It should be noted that

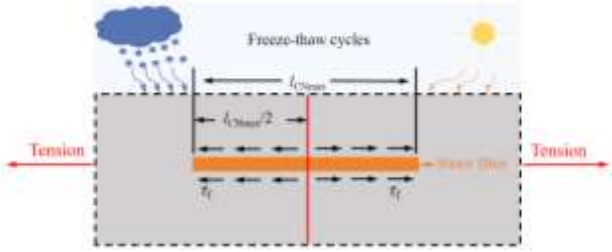

Fig. 12 Schematic of the method for determining critical straw fiber length

this study assumes fibers are arranged linearly within the soil, whereas in practical engineering applications, fibers are generally randomly distributed. Random orientation introduces effects including varying orientation angles, local bending, and overlapping, which can influence the tensile and pull-out performance of the fibers. In particular, for relatively long fibers, random distribution tends to promote bending and twisting within the soil, leading to a shorter average effective length and a critical fiber length that may exceed those obtained in this study. Therefore, in practical design, it is advisable to moderately increase the fiber length to account for the effects of random orientation. Future research could further explore interfacial behavior under random fiber distributions using three-dimensional numerical simulations or other appropriate methods. Moreover, the laboratory simulations use idealized thermal cycles (−20°C to 20°C), whereas field conditions involve slower, irregular temperature changes driven by environmental factors, resulting in complex interfacial interactions between fibers and the surrounding soil. Therefore, further research is necessary to more accurately characterize and refine the critical straw fiber length, ultimately enhancing the design reliability of straw fiber-reinforced frozen soils under practical freeze-thaw conditions.

In summary, this study emphasizes the critical role of freeze-thaw cycles in governing the mechanical behavior of fiber-soil interfaces, an aspect often overlooked in previous research, which primarily focuses on fiber morphology or surface roughness (Singh *et al*. 2004, Vincenzini *et al*. 2021, Yao *et al*. 2024). Single-fiber pull-out tests provide quantitative characterization of interfacial degradation at the macroscopic scale. Complementary SEM and NMR analyses further elucidate the underlying deterioration mechanisms, highlighting the connection between pore structure evolution and interfacial failure. Moreover, a critical fiber length under freeze-thaw conditions is newly proposed and quantified. This design-oriented parameter extends the theoretical framework for assessing reinforcement effectiveness and offers practical guidance for engineering applications in cold regions. By integrating macroscopic testing, microscopic observations, and quantitative modeling, this study enhances the mechanistic understanding of fiber-soil interface behavior and provides valuable insights for predicting durability and ensuring the long-term performance of fiber-reinforced soils under freeze-thaw conditions.

6. Conclusions

This study comprehensively investigated the effects of freeze-thaw cycles on straw fiber-soil interfacial strength. A series of single-fiber pull-out, SEM, and NMR tests were conducted after 0, 1, 3, 5, 10, 15, and 20 freeze-thaw cycles. Based on the test results, the main conclusions are summarized as follows:

(1) The pull-out load-displacement response of the straw fiber is primarily governed by the mechanical properties of the fiber-soil interface, while freeze-thaw cycles have little impact on the overall curve shape.

(2) Both the fiber-soil interfacial cohesion and friction angle decrease exponentially with the number of freeze-thaw cycles, and their degradation can be estimated by the proposed semi-empirical equation.

(3) Fiber-soil interfacial strength degradation under freeze-thaw conditions is exacerbated by higher water content or greater dry density. SEM and NMR analyses reveal a positive correlation between the degree of degradation and pore development, which becomes more pronounced under these conditions.

(4) Based on the interfacial strength measured from single-fiber pull-out tests, a calculation method for the critical fiber length in straw fiber-reinforced frozen soils is developed, providing a basis for engineering design under freeze-thaw conditions.

Acknowledgements

This study is supported by the National Natural Science Foundation of China (52478364).

References

Ali M., Aziz, M., Hamza, M. and Madni, M.F. (2020), "Engineering properties of expansive soil treated with polypropylene fibers", *Geomech. Eng.*, **22**(3), 227-236. https://doi.org/10.12989/gae.2020.22.3.227.

Bag, R. and Jadda, K. (2021), "Influence of water content and dry density on pore size distribution and swelling pressure of two Indian bentonites", *Bull. Eng. Geol. Environ.*, **80**, 8597-8614. https://doi.org/10.1007/s10064-021-02459-0.

Bahrami, M. and Marandi, S.M. (2020), "Effect of strain level on strength evaluation of date palm fiber-reinforced sand", *Geomech. Eng.*, **21**(4), 327-336. https://doi.org/10.12989/gae.2020.21.4.327.

Bo, L., Li, Z., Li, P., Xu, G., Xiao, L. and Ma, B. (2021), "Soil freeze-thaw and water transport characteristics under different vegetation types in seasonal freeze-thaw areas of the loess plateau", *Front. Earth Sci.*, **9**, 704901. https://doi.org/10.3389/feart.2021.704901.

Bozyigit, I. (2025), "Strength properties of clay treated with fiber and biopolymer subject to freeze-thaw conditions", *J. Mater. Civ. Eng.*, **37**(5), 04025090. https://doi.org/10.1061/JMCEE7.MTENG-19201.

Chen, Y. (2018), "Soil-water retention curves derived as a function of soil dry density", *GeoHazards*, **1**(1), 3-19. https://doi.org/10.3390/geohazards1010002.

Cheng, S., Wang, Q., Fu, H., Wang, J., Han, Y., Shen, J. and Lin, S. (2021), "Effect of freeze-thaw cycles on the mechanical properties and constitutive model of saline soil", *Geomech. Eng.*, **27**(4), 309-322. https://doi.org/10.12989/gae.2021.27.4.309.

Dang, L. C., Fatahi, B. and Khabbaz, H. (2016), "Behaviour of expansive soils stabilized with hydrated lime and bagasse fibres", *Procedia Eng.*, **143**, 658-665. https://doi.org/10.1016/j.proeng.2016.06.093.

Deng, Y., Yue, X., Liu, S., Chen, Y. and Zhang, D. (2015), "Hydraulic conductivity of cement-stabilized marine clay with metakaolin and its correlation with pore size distribution", *Eng. Geol.*, **193**, 146-152. https://doi.org/10.1016/j.enggeo.2015.04.018.

Güllü, H. and Khudir, A. (2014), "Effect of freeze-thaw cycles on unconfined compressive strength of fine-grained soil treated with jute fiber, steel fiber and lime", *Cold Reg. Sci. Technol*., **106**, 55-65. https://doi.org/10.1016/j.coldregions.2014.06.008.

Hejazi, S.M., Sheikhzadeh, M., Abtahi, S.M. and Zadhoush, A. (2012), "A simple review of soil reinforcement by using natural and synthetic fibers", *Constr. Build. Mater.*, **30**, 100-116. https://doi.org/10.1016/j.conbuildmat.2011.11.045.

Ji, X.D., Cong, X., Dai, X.Q., Zhang, A. and Chen, L.H. (2018), "Studying the mechanical properties of the soil-root interface using the pullout test method", *J. Mount. Sci.*, **15**(4), 882-893. https://doi.org/10.1007/s11629-015-3791-4.

Kafodya, I. and Okonta, F. (2021), "Effect of fibre surface coating on the mechanical properties of natural fibre-reinforced soil", *Int. J. Geotech. Eng.*, **15**(3), 338-348. https://doi.org/10.1080/19386362.2018.1542557.

Kakroudi, H. A., Bayat, M. and Nadi, B. (2024), "Static and dynamic characteristics of silty sand treated with nano-silica and basalt fiber subjected to freeze-thaw cycles", *Geomech. Eng.*, **37**(1), 85-95. https://doi.org/10.12989/gae.2024.37.1.085.

Kravchenko, E., Liu, J., Krainiukov, A. and Chang, D. (2019), "Dynamic behavior of clay modified with polypropylene fiber under freeze-thaw cycles", *Transp. Geotech.*, **21**, 100282. https://doi.org/10.1016/j.trgeo.2019.100282.

Kumar, K. R., Gobinath, R., Shyamala, G., Viloria, E. and Varela, N. (2020), "Free thaw resistance of stabilized and fiber-reinforced soil vulnerable to landslides", *Materials Today: Proceedings*, **27**, 664-670. https://doi.org/10.1016/j.matpr.2020.02.041.

Lee, Y., Kang, S.T. and Kim, J.K. (2010). "Pullout behavior of inclined steel fiber in an ultra-high strength cementitious matrix", *Constr. Build. Mater.*, **24**(10), 2030-2041. https://doi.org/10.1016/j.conbuildmat.2010.03.009.

Li, T., Kong, L. and Liu, B. (2020), "The California bearing ratio and pore structure characteristics of weakly expansive soil in frozen areas", *Appl. Sci.*, **10**(21), 7576. https://doi.org/10.3390/app10217576.

Li, Y., Ling, X., Su, L., An, L., Li, P. and Zhao, Y. (2018), "Tensile strength of fiber reinforced soil under freeze-thaw condition", *Cold Reg. Sci. Technol.*, **146**, 53-59. https://doi.org/10.1016/j.coldregions.2017.11.010.

Liu, C., Lv, Y., Yu, X. and Wu, X. (2020), "Effects of freeze-thaw cycles on the unconfined compressive strength of straw fiber-reinforced soil", *Geotext. Geomembranes*, **48**(4), 581-590. https://doi.org/10.1016/j.geotexmem.2020.03.004.

Monazami, M. and Gupta, R. (2022), "Effect of curing age on pull-out response of carbon, steel, and synthetic fiber embedded in cementitious mortar matrix", *J. Mater. Civil. Eng.*, **34**(10), 04022275. https://doi.org/10.1061/(ASCE)MT.1943-5533.0004426.

Orakoglu, M.E. and Liu, J. (2017), "Effect of freeze-thaw cycles on triaxial strength properties of fiber-reinforced clayey soil", *KSCE J. Civ. Eng.*, **21**(6), 2128-2140. https://doi.org/10.1007/s12205-017-0960-8.

Oulapour, M., Adib, A. and Safii, A. (2025), "Enhancing strength

and durability of fine-grained soils with persian gum biopolymer and glass fibers under freeze-thaw cycles", *Geotech. Geol. Eng.*, **43**, 200. https://doi.org/10.1007/s10706-025-03179-y.

Shannag, M.J., Brincker, R. and Hansen, W. (1997), "Pullout behavior of steel fibers from cement-based composites", *Cement. Concret. Res.*, **27**(6), 925-936. https://doi.org/10.1016/S0008-8846(97)00061-6.

Singh, S., Shukla, A. and Brown, R. (2004), "Pullout behavior of polypropylene fibers from cementitious matrix", *Cement. Concret. Res.*, **34**(10), 1919-1925. https://doi.org/10.1016/j.cemconres.2004.02.014.

Sun, Y., Shi, J., Liu, Z., Liu, C. and Zhang, Y. (2024). "The failure modes of flexible fibers in reinforced soil with different dry densities", *Constr. Build. Mater.*, **449**, 138386. https://doi.org/10.1016/j.conbuildmat.2024.138386.

Tang, C.S., Shi, B. and Zhao, L.Z. (2010), "Interfacial shear strength of fiber reinforced soil", *Geotext. Geomembranes.*, **28**(1), 54-62. https://doi.org/10.1016/j.geotexmem.2009.10.001.

Tang, C.S., Wang, D.Y., Cui, Y.J., Shi, B. and Li, J. (2016), "Tensile strength of fiber-reinforced soil", *J. Mater. Civil. Eng.*, **28**(7), 04016031. https://doi.org/10.1061/(ASCE)MT.1943-5533.0001546.

Tang, L., Du, Y., Liu, L., Jin, L., Yang, L. and Li, G. (2020), "Effect mechanism of unfrozen water on the frozen soil-structure interface during the freezing-thawing process", *Geomech. Eng.*, **22**(3), 245-254. https://doi.org/10.12989/gae.2020.22.3.245.

Tian, H., Wei, C., Wei, H., Yan, R. and Chen, P. (2014), "An NMR-based analysis of soil-water characteristics", *Appl. Mag. Reson.*, **45**, 49-61. https://doi.org/10.1007/s00723-013-0496-0.

Toufigh, V., Saeid, F., Toufigh, V., Ouria, A., Desai, C.S. and Saadatmanesh, H. (2014), "Laboratory study of soil-CFRP interaction using pull-out test", *Geomech. Geoeng.*, **9**(3), 208-214. https://doi.org/10.1080/17486025.2013.813650.

Vakili, A. H., Salimi, M., Lu, Y., Shamsi, M. and Nazari, Z. (2022), "Strength and post-freeze-thaw behavior of a marl soil modified by lignosulfonate and polypropylene fiber: an environmentally friendly approach", *Constr. Build. Mater.*, **332**, 127364. https://doi.org/10.1016/j.conbuildmat.2022.127364.

Vincenzini, A., Augarde, C.E. and Gioffrè, M. (2021), "Experimental characterization of natural fibre-soil interaction: Lessons for earthen construction", *Mater. Struct.*, **54**(3), 110. https://doi.org/10.1617/s11527-021-01703-z.

Wang, L., Wang, H., Tian, Z., Lu, Y., Gao, W. and Ren, T. (2020), "Structural changes of compacted soil layers in northeast china due to freezing-thawing processes", *Sustainability*, **12**(4), 1587. https://doi.org/10.3390/su12041587.

Xu, M. (2022), "Study on mechanical properties of straw fiber and its reinforced saline soil by freeze-thaw action", Master's Thesis, Anhui University of Science and Technology, Huainan city, China. (in Chinese).

Yan, C., An, N., Wang, Y. and Sun, W. (2021), "Effect of dry-wet cycles and freeze-thaw cycles on the antierosion ability of fiber-reinforced loess", *Adv. Mater. Sci. Eng.*, **2021**(1), 8834598. https://doi.org/10.1155/2021/8834598.

Yang, Z., Lu, Z., Shi, W., Ling, X., Liu, X., Guan, D. and Zhang, J. (2024), "Effects on the micropore structure and unfrozen water content in expansive soil under freeze-thaw cycles via low-field NMR", *Geomech. Geoeng.*, **19**(5), 705-720. https://doi.org/10.1080/17486025.2024.2304703.

Yao, X., Xu, Y., Dong, X. and Tian, Z. (2024), "Assessing the desiccation crack propagation performance of cemented soil reinforced by modified polyvinyl alcohol fiber", *Measurement*, **235**, 114920. https://doi.org/10.1016/j.measurement.2024.114920.

Yu, X., Wu, X., Zhu, P., Liu, C., Qiu, C. and Cai, Z. (2025), "Mechanism of strength degradation of fiber-reinforced soil under freeze-thaw conditions", *Buildings*, **15**(6), 842. https://doi.org/10.3390/buildings15060842.

Zaimoglu, A.S., Akbulut, R.K. and Arasan, S. (2016), "Effect of freeze-thaw cycles on strength behavior of compacted chicken quill-clay composite in undrained loading", *J. Nat. Fibers*, **13**(3), 299-308. https://doi.org/10.1080/15440478.2015.1029188.

Zhu, H., Zhang, C., Tang, C., Shi, B. and Wang, B. (2014), "Modeling the pullout behavior of short fiber in reinforced soil", *Geotext. Geomembranes*, **42**(4), 329-338. https://doi.org/10.1016/j.geotexmem.2014.05.005.

JS